Ceramics-Silikáty 66 (4), 480-488 (2022)
www.ceramics-silikaty.cz doi: 10.13168/cs.2022.0044

EFFECT OF THE $CaO–MgO–Al_2O_3–SiO_2$ GLASS COMPOSITION ON THE MICROSTRUCTURE AND RHEOLOGICAL PROPERTIES FROM A MOLECULAR DYNAMICS SIMULATION

[#]GU GUOXUAN*, LI SHENG**, LIU XIN*, YANG SHENGYUN*, CAO YI***, QU YA*, LIANG XUNMEI****, CHEN XIANJING*****, [#]YUE YUNLONG*, [#]KANG JUNFENG*

*School of Materials Science and Engineering, University of Jinan, Jinan 250022, China
**Qingyuan CSG new energy-saving materials Co. Ltd, Qingyuan 511500, China
***School of Information Science and Engineering, University of Jinan, Jinan 250022, China
****Shandong Road New Materials Co. Ltd, Taian 271000, China;
*****Shandong Institute for Product Quality Inspection, Jinan, 250102, China

[#]E-mail: zztg_yueyl@163.com, mse_kangjf@ujn.edu.cn

Submitted August 23, 2022; accepted September 26, 2022

Keywords: Molecular dynamics simulation, Glassy melts, Viscosity, Fragility, Structure

By adjusting the ratio of SiO_2/RO (R=Ca, Mg), this article studied the atomic structure of $CaO–MgO–Al_2O_3–SiO_2$ glassy melts by a molecular dynamics simulation. The Pair distribution function (PDF), Coordination number (CN), bridging oxygen (BO), non-bridging oxygen (NBO), and Qn were utilised to characterise the glass structure. The results indicated that the content of the bridging oxygen was decreased with the RO replacing the SiO_2. The total content of Q4 in the tetrahedron changed significantly from 34.11 % to 18.06 %. Meanwhile, the NBO/T parameter increased from 1.298 to 1.555. In the corresponding viscosity test, the melting temperature, fitted by the MYEGA equation, also decreased with the decrease in the SiO_2 content, and the fragility value increased from 39.12 to 53.20. Finally, the fragility and NBO/T were linked to describing the relationship between the mid-range structure and the rheological property. Moreover, the analyses showed that they had a linear relationship.

INTRODUCTION

$CaO–MgO–Al_2O_3–SiO_2$ glasses are widely used in glass ceramics and high strength and high modulus glass fibre fields [1, 2]. Nevertheless, all of them have high melting temperatures, which can bring about difficulties for the manufacturing processes. In order to decrease the melting temperatures, many people have studied the high-temperature rheological properties, structural evolution of glass melts, and so on. J. Y. Cavaille et al. [3] proposed a theory for the rheology of the glassy state, stating that internal defects in glasses could cause large shear deformation at a high temperature, which could lead to irrecoverable structural deformation. Yue et al. [4] found that the fragility of CaO–MgOŞAl_2O_3–SiO_2 glass melts reached the minimum value when Ca/ /(Ca+Mg) was equal to 0.5, reflecting the mixed alkaline-earth effect. The reason for this phenomenon was that the tetrahedral connections around the network modifier ions became weakened where plastic flow also occurred, which reduced the fragility [5, 6]. Charles Le Losq et al. [7] reported the role of Al^{3+} on the rheology and structural changes in glasses and melts. They suggested that the content of a fivefold coordination of Al^{3+} ions increased with an increase in the temperature. All in all, the studies just concentrated on the changes in the rheology and structure around T_g (the glass-transition temperature), and there have been few studies on the relationship between the rheological properties and the glass structures at the melting temperature.

It is difficult to obtain the structures of the glass melts directly from experiments in the current conditions, thus, the molecular dynamic (MD) simulations have gradually been favoured by researchers [8, 9]. Back in the 1970s, Woodcock et al. [10] studied the MD simulation of silica glass. Thomas F. Soules et al. [11] used an MD simulation to study the rheological properties of sodium silicate glass. In their research, the mobility of silicon atoms and oxygen atoms under stress was poor at low temperatures. M. Bauchy [12] reported that the changes in the number of Na atoms led to a change in the polymerisation degree of the glass network at an ambient pressure. Nguyen VanHong et al. [13] discussed that Ca ions were usually bound to the glass network structure by providing a non-bridging oxygen and by balancing negative charges. Li et al. [14-17] reported the influence of CaO and MgO in the melt of the $CaO–MgO–Al_2O_3–SiO_2$ system. They observed that MgO was more likely to destroy the glass structure than CaO. Jiang et al. [15] studied the depolymerisation of the glass network resulting from changes in the Mg/Al ratio. Similar results were also observed with the changes in the Ca/Si ratio [18]. In general, there have been extensive studies on MD simulations in glasses, with detailed studies covering the structures and properties [19-21]. Nevertheless, the rheological properties of experiments at the melting temperature are inconclusive with the simulated structure.

Based on the change of the SiO_2/RO ratio in the CaO–MgO–Al_2O_3–SiO_2 system, the structures of high-temperature melts were simulated through the MD simulation, and viscosity models were applied to obtain the melting temperature and fragility. Then the impact of the structures on these properties was discussed. Finally, the relationship between the fragility and NBO/T is also discussed in this paper.

EXPERIMENTAL

Glass compositions

In this article, the structure and viscosity of CaO–MgO–Al_2O_3–SiO_2 (CMAS) glasses at high temperatures were studied by adjusting the SiO_2/RO ratio. These compositions are shown in Table 1 with the addition of Na_2O to reduce the melting temperature. Three-hundred-gram (300 g) glass batches were melted in a platinum crucible for 4 ~ 6 h in the air at 1600 ~ 1650 °C. After ensuring that the materials were fully melted, the glass melts were poured into the plaster mould and then annealed at 750 ~ 850 °C, depending on the glass compositions. The resulting glass samples were used for the viscosity testing. The raw materials were as follows: SiO_2 (analytical pure 99.99 %), Al_2O_3 (analytical pure 99.99 %), CaO (analytical pure 99.99 %), MgO (analytical pure 99.99 %), and Na_2CO_3 (analytical pure 99.99 %).

Table 1. Glass compositions of the CMAS *x*-*y* glasses (*x*CaO–*y*MgO–20Al_2O_3–(79–*x*–*y*)SiO_2 ($x = y$ = 6, 7, 8, 9, 10, 11)).

Group number	Composition (mol. %)				
	Na_2O	CaO	MgO	Al_2O_3	SiO_2
1	1	6	6	20	67
2	1	7	7	20	65
3	1	8	8	20	63
4	1	9	9	20	61
5	1	10	10	20	59
6	1	11	11	20	57

Potential function

The choice of the potential function is the most important step in the molecular dynamics simulation. Whether the results of the simulation are accurate or not is often related to this. We opted for the potential function of the Born-Mayer-Huggins potential [22]:

$$U_{ij}(r_{ij}) = \frac{q_i q_j}{4\pi\varepsilon_0 r_{ij}} + f_0(b_i + b_j)\exp\left(\frac{(a_i + a_j) - r_{ij}}{b_i - b_j}\right) - \frac{C_i C_j}{r_{ij}^{\ 6}} + \frac{D_i D_j}{r_{ij}^{\ 8}} \quad (1)$$

where *a*, *b*, *C*, and *D* are the fitting parameters that change as the material changes. $U_{ij}(r_{ij})$ is the total energy of the forces around each atom; r_{ij} is the distance of atoms *i* and *j*; f_0 is the standard force parameter, in which it is selected for 0.0424 eV/Å; q_i and q_j represent the effective charge of atoms *i* and *j*, respectively. The function, on the right-hand side, has three parts: the first is the Coulombic interactions; the second is the short-range electronic repulsion; the third is the Van der Waals force parameters.

In this paper, the atom partial charges were as follows: $| q_{Ca} | = | q_{Mg} | = | q_O | = 0.5| q_{Si} | = 0.67| q_{Al} | = 2| q_{Na} | = 0.945$ eV. The parameters chosen to be used in this paper (Table 2) were proposed by Mutsui [23] and improved by Jabraoui [24] in 2018 due to their good performance in the structural simulation of alumina silicate glass.

Simulation procedures

A LAMMPS [25] (Large-scale Atomic/Molecular Massively Parallel Simulator) was used in this paper. Glass models randomly placed the Si, Al, Ca, Mg, Na, and O atoms that included 8065 atoms in these units. The Verlet algorithm was used in this paper for the differential motion equations. The timestep was 1 fs and the cut-off was 12 Å. These units were first energy minimised at 0 K and then relaxed at 300 K for 30 ps. Afterward, these units were melted at 5000 K for 100 ps. The above processes all used the constant temperature, constant volume (NVT) ensemble. Hereafter, these units were cooled down to the melting temperature for 30 ps and they were relaxed using the NVT ensemble and the constant temperature, constant pressure (NPT) ensemble at this temperature. These units also used the same steps to 300 K. The cooling processes were all carried out at a cooling rate of 5×10^{-3} K/fs based on previous research [26-28]. This article mainly studied the structural changes at the melting temperature.

Table 2. Parameters of the interatomic potential.

	$A = f_0(b_i + b_j)$ (eV/Å)	$(b_i + b_j)$ (Å)	$(a_i + a_j)$ (Å)	$C = c_i c_j$ (eV/Å^6)	$D = D_i D_j$ (eV/Å^{12})
Si–O	0.0070	0.1560	2.5419	46.29	0
Al–O	0.0073	0.1640	2.6067	34.57	0
Ca–O	0.0077	0.1780	2.1935	40.26	0
Mg–O	0.0077	0.1780	2.7155	27.28	0
Na–O	0.0077	0.1780	2.1419	38.42	0
O–O	0.0120	0.2630	3.6430	85.08	0

Structural analysis methods

Pair distribution function and Coordination numbers

The pair distribution function (PDF) is a necessary method to describe the glass structure. PDF characterises the probability for a kind of atom around the central atom. The PDF can be described through the following equation [29]:

$$g_{ij}(r) = \frac{V}{N_i N_j} \sum_j \frac{n(r)}{4\pi r^2 \Delta r} \qquad (2)$$

where, r is the distance of the i and j ions; N_i and N_j are the number of i and j ions, respectively; V is the volume of these units; $n(r)$ is the average number of j ions within the radius of the spherical shell around ion i in the region between r and $r \pm \Delta r/2$.

The coordination numbers (CN) represent the number of other atoms around an atom within a specific radius. The CN is shown by the following equation [30, 31]:

$$N_{ij}(r) = \frac{4\pi N_j}{V} \int_0^r g_{ij}(r)\, r^2\, dr \qquad (3)$$

where $N_{ij}(r)$ represents numbers of j ions within radius r around ion i; N_j is the number of j atoms, V is the volume of these units; $g_{ij}(r)$ is the PDF of ions i and j.

Bridging oxygen and non-bridging oxygen

The bridging oxygen and non-bridging oxygen (BO and NBO) indicate the oxygen ions connection status in the glass former. Oxygen ions play three main roles in the glass structure, which are called the bridging (connected to two network structural units), non-bridging (only connected to one network structural unit), and free oxygen (FO, not connected to any network structural unit). The content of BO, NBO, and FO was counted by an original python code.

Q^n distribution

Aluminosilicate glass network is constituted of different tetrahedrons (network structure units), such as $[SiO_4]$, $[AlO_4]$, and so on. In this paper, Q^n is used to describe the connection between these tetrahedrons, where Q is the network forming body in the glass and n is the number of bridging oxygen per unit. Q^n can describe the medium-range structure and the degree of the order of the glass [32].

Rheological property characterisation methods

Viscosity

The high-temperature viscosity of the CMAS glass melts was measured with a viscometer (the model of Orton RSV-1600). In this paper, 300 g of the melted glass was placed into the viscosimeter and the furnace atmosphere was set to the atmosphere of air (1 GPa). Then the temperature range was set between 1623 K and 1853 K. After being heated to 1853 K, the temperature was cooled to 1623 K at a cooling rate of 2 K·min^{-1}. Finally, the viscosity and temperature data were outputted.

Glass transition temperature

The glass transition temperature (T_g) was measured by a Model 1412 STD Dilatometer. In this paper, the glass sample (4 × 4 × 25.4 mm) was put into the instrument and the test temperature range was set from room temperature to 1173 K at a rate of 5 K·min^{-1}. The recorded thermal expansion curve was used to obtain the T_g.

MYEGA equation

John C. Mauro and co-workers connected the relationship between T_g and m (the fragility) and rewrote the MYEGA equation as [33]:

$$\log_{10}\eta_\infty = \log_{10}\eta_\infty + (12 - \log_{10}\eta_\infty)\,\frac{T_g}{T}\,\exp \exp\left[\left(\frac{m}{12 - \log_{10}\eta_\infty} - 1\right)\left(\frac{T_g}{T} - 1\right)\right] \qquad (4)$$

RESULTS AND DISCUSSIONS

Structural analysis

Pair distribution function and Coordination number analysis

Figure 1 shows the PDF and CN for group 3. As shown in Figure 1a, the first peak of $g_{Si–O}(r)$ is 1.63Å. In contrast to the other peaks, the first peak of $g_{Si-O}(r)$ is the leftmost and its peak intensity is the highest, which means that the most likely bonding trend is between the silicon atoms and oxygen atoms [34-36]. The Al–O bond length is 1.73Å, which is in agreement with the previous results of MD simulations for sodium aluminosilicate glasses [30]. The first peak of $g_{Ca-O}(r)$ and $g_{Mg-O}(r)$ is 2.42 Å and 1.96 Å, respectively. The Mg–O bond length is shorter than the Ca–O bond length because Mg^{2+} has a smaller radius and greater field strength than Ca^{2+}, and Mg^{2+} has a stronger effect on the oxygen ions accumulation [14, 37-39]. The bond length of Na–O is 2.37 Å, and the Na–O bond length obtained by Extended X-ray absorption fine structure (EXAFS) is 2.32 Å [40], demonstrating that the simulated result is close to the real experimental values. The O–O bond length is 2.65 Å, and the result is very close to the neutron diffraction result (2.63 Å) [41].

The coordination numbers are obtained by integrating $g(r)$ to characterise the connection between the ions. The CNs between various ions and oxygen ions are exhibited in Figure 1b. The CN of Si–O indicates that most silicate ions form $[SiO_4]$ units in the glass, with an average value of 4.049. This is consistent with the results obtained from the Nuclear magnetic resonance (NMR) spectroscopy experiment [42]. Compared with Si–O, the CN platform of Al–O is leaner as Al has five/six coordinations in the glass network [30]. The other ions have no distinct platform, which is consistent with the result of Jiang [14].

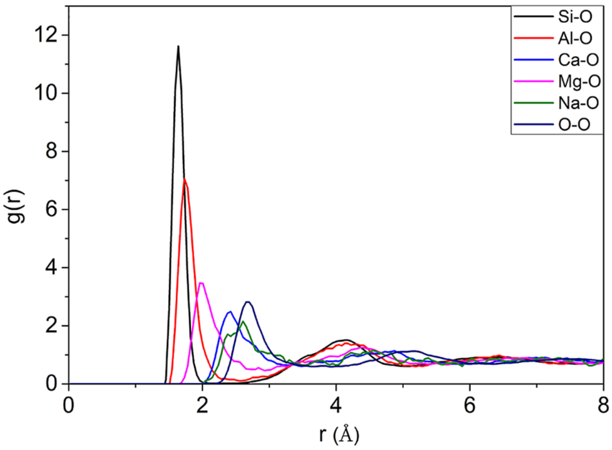

a)

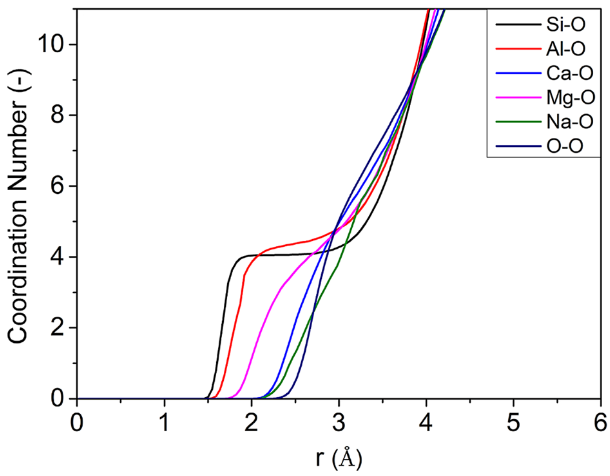

b)

Figure 1. Pair distribution function (a) and Coordination number (b) analysis of Group 3.

The CNs of Si–O and Al–O in groups 1-6 are listed in Table 3. It can be observed that the CNs of Si–O and Al–O increase with the addition of CaO and MgO. However, the CN of Al–O is more affected than the CN of Si-O. This also indicates that the Si–O bond is stronger than the Al–O bond [15].

Table 3. The CNs of Si–O and Al–O.

Group number	1	2	3	4	5	6
$CN_{Si–O}$	4.014	4.026	4.049	4.068	4.078	4.090
$CN_{Al–O}$	4.031	4.065	4.084	4.132	4.135	4.206

Bridging oxygen and non-bridging oxygen

The BO and NBO characterising the oxygen species around Si and Al atoms are shown in Figure 2. As shown in Figure 2a, the variation of the oxygen species around Si atoms is obvious. The BO content decreases from 84.5 % to 64.0 % and the NBO content increases from 15.2 % to 35.0 % when SiO_2 is replaced by CaO and MgO. The FO content also increases from 0.3 % to 1.0 %. As shown in Figure 2b, the variation in the oxygen species around the Al atoms is similar to the Si atoms. The BO content declines from 86.3 % to 66.0 %, and the NBO content of rises from 13.5 % to 32.8 %, while the FO content increases from 0.2 % to 0.9 %. All this indicates that the introduction of alkaline earth metal ions results in breaking bonds between the glass units, and causes a trend in the transformation of BO to NBO [16], leading to an increase in the degree of the disorder for the glass. Hence, the glass network becomes depolymerised, leading to a decrease in the high-temperature viscosity [43], which will be discussed below.

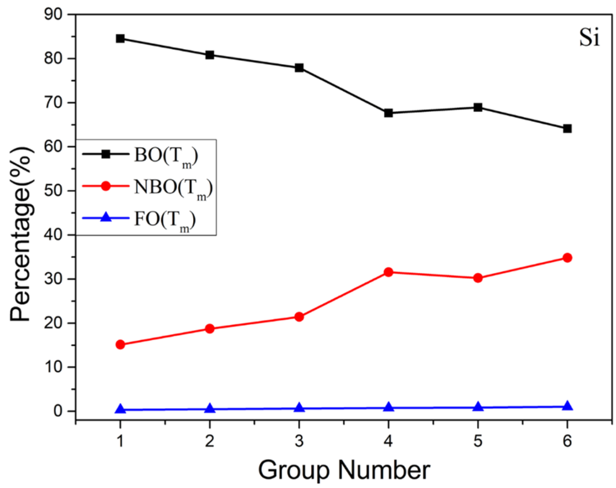

a) Si atoms

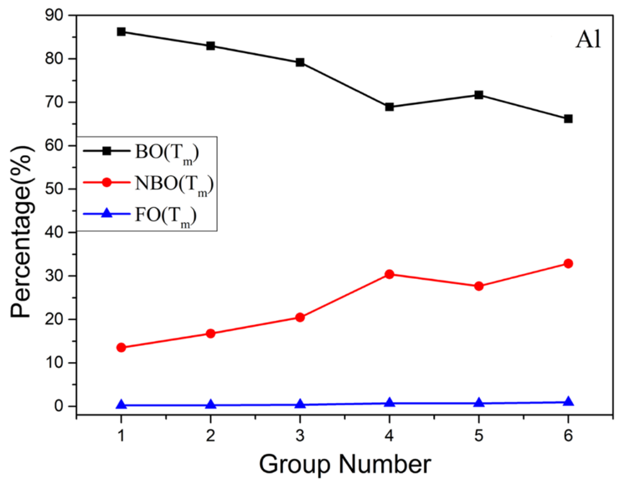

b) Al atoms

Figure 2. Bridging oxygen and non-bridging oxygen of the Si atoms (a) and Al atoms (b).

Q^n distribution

The Q^n distribution of $[SiO_4]$ and $[AlO_4]$ is demonstrated in Figure 3a and b, respectively. From group 1 to group 6, the Q^4 content of the silicon ions declines visibly from 37.65 % to 16.57 %, and the Q^2 and Q^1 content increases monotonically. Meanwhile, Q^3 and Q^0 do not change significantly. The phenomenon with the highest Q^3 content is also observed in sodium silicate glass [41] and has been verified by NMR and Raman spectra [44, 45]. Compared with silicon, the Q^3 and Q^2 content from aluminium ions clearly rises. The Q^3 content changes from 25.00 % to 32.99 %. At the same time, Q^4, Q^1, and Q^0 distinctly decline. The Q^n distribution change of the Al accords with the disproportionation reaction: $2Q^3Q^2+Q^4$. The addition of alkaline earth metal ions makes the disproportionation reaction proceed to the left, which also confirms the destruction of the structure by alkaline earth metal ions [41].

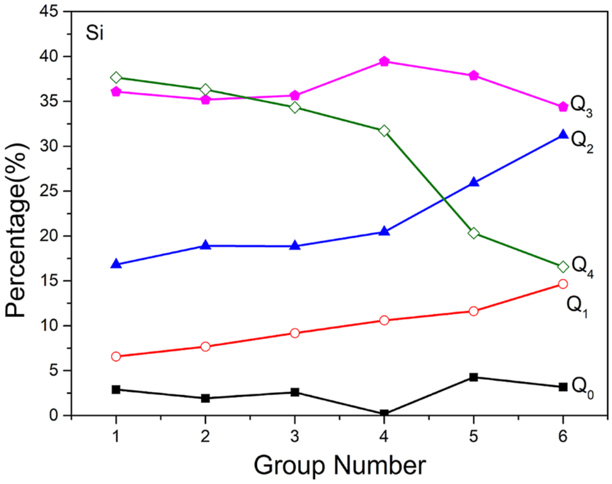

a) SiO_4

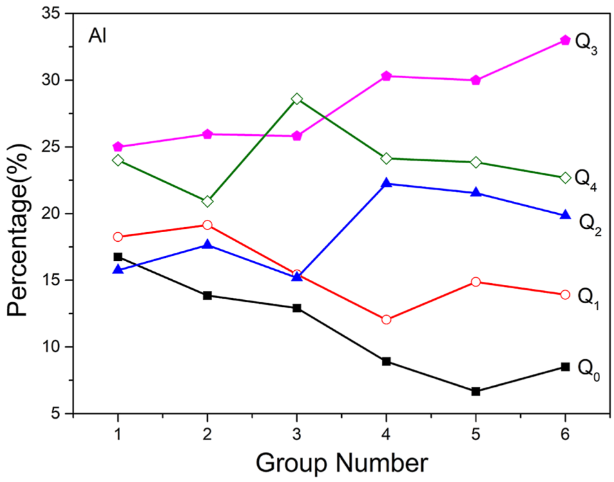

b) AlO_4

Figure 3. Qn distribution of SiO_4 (a) and AlO_4 (b).

NBO/T and BO/T

Norimasa et al. studied the structure of alkali silicate glass and melting by Raman spectra, introducing an NBO/Si equation [46]:

$$\frac{NBO}{Si} = \sum_{i=1}^{3} X_i n_i \tag{5}$$

where n_i is the number of NBO in $[SiO_4]$, X_i is the mole fraction of Q^n.

Based on this, the structural parameter is calculated in this paper:

- The average number of NBO in each tetrahedron (NBO/T):

$$\frac{NBO}{T} = \frac{\sum Q^n \times (4-n)}{[Si]+[Al]} \tag{6}$$

- The average number of BO in each tetrahedron (BO/T):

$$\frac{BO}{T} = \frac{\sum Q^n \times n}{[Si]+[Al]} \tag{7}$$

in these formulas, T represents the number of tetrahedra in the glass network, Q^n is the content of each tetrahedron, n is the number of Bridging oxygen that can connect to other tetrahedrons in each Q^n, and [Si]+[Al] is the number of silicon and aluminium atoms.

The relationship between the NBO/T and BO/T is shown in Figure 4 and the specific values are listed in Table 4. The increase in the NBO/T and the decrease in the BO/T can be explained by the addition of alkali earth metal cations: The atomic density of glass decreases gradually with an increase in the CaO and MgO content in the glass components, which also results in a decrease in the polymerisation degree of the glass network [5]. Moreover, alkaline earth metal cations break the tetrahedral connections by breaking bonds, and then they are added to the glass network by providing NBO [47], ultimately reducing the BO content and increasing the NBO content. Thus, the rise in the NBO/T indicates the depolymerisation of the glass structure [48].

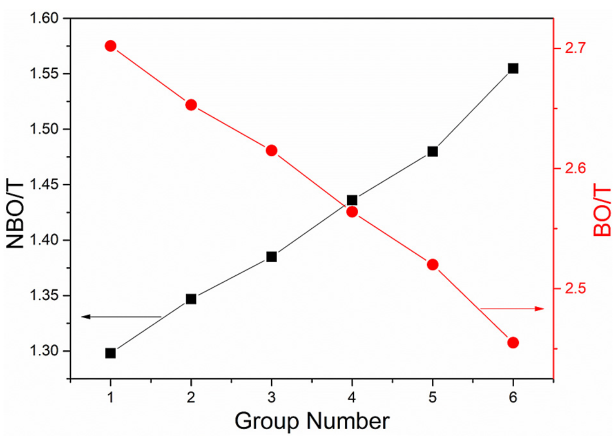

Figure 4. NBO/T and BO/T calculated by Equations 6 and 7.

Table 4. NBO/T and BO/T values for the different glass samples.

Group number	1	2	3	4	5	6
NBO/T	1.30	1.34	1.39	1.44	1.48	1.56
BO/T	2.70	2.65	2.62	2.56	2.52	2.46

Rheological property analysis

High-temperature viscosity

Furthermore, the glass viscosity was measured in this paper. Figure 5 shows the fitting results of the glass viscosity by using the MYEGA equation combined with high-temperature viscosity and T_g. Moreover, the melting temperature obtained by the MYEGA equation is listed in Table 5. It is visible that the viscosity and the melting temperature of the glasses decrease with the replacement of SiO_2 with CaO and MgO. For reference, an increase in the MgO content leads to a decrease in the high-temperature viscosity in the CaO–SiO_2–Al_2O_3––MgO slag [49]. MgO provides excess oxygen ions and depolymerises the structure into small structural units. Likewise, CaO has similar properties that CaO can significantly promote the transition of BO to NBO [18]. Alkaline earth metal cations in the glass melt move freely at high temperatures and cause the polarisation of oxygen ions, thereby reducing the melt viscosity and the melting temperature [50]. With an increase in the Ca and Mg ions in the glass system, the oxygen ion polarisation rate increases. This leads to the weakening or even breaking of the Si–O bond, and finally depolymerisation of the glass structure.

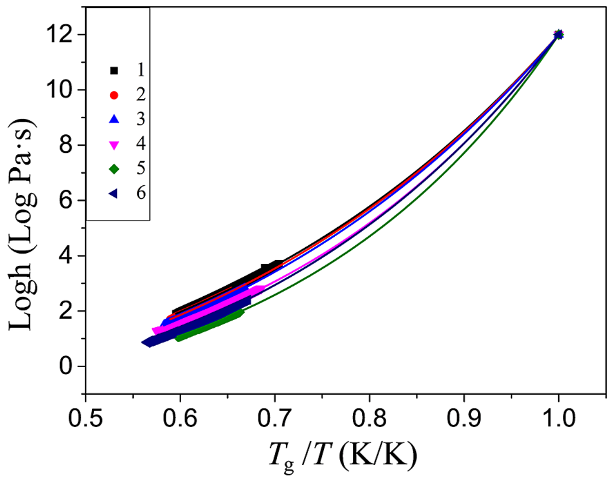

Figure 5. Temperature dependence of the viscosity with the MYEGA equation.

Table 5. The melting temperature of fitting by the MYEGA equation.

Group number	1	2	3	4	5	6
Temp. (K)	2030.6	1972.1	1917.6	1897.0	1761.8	1723.2

Fragility

C.A. Angell proposed that glass melts with a deviation from linear viscosity versus temperature are called fragile liquids [51]. In this paper, the glass fragility, based on the high-temperature viscosity data, is fitted by the MYEGA equation. As shown in Figure 6, the glass fragility value increases monotonically from 39.12 to 53.20 while the components of SiO_2 decrease. Hajinme proposed the magnitude of the fragility is related to the medium-range structure of the glass [52]. So, the increase in fragility is attributed to the decrease in the BO content and the increase in the NBO content. Meanwhile, the decrease in the total Q^4 content is also the reason for the fragility growth. This indicates that the increase in the fragility means the depolymerisation of the glass structure at high temperatures [53]. It is also consistent with the simulation results.

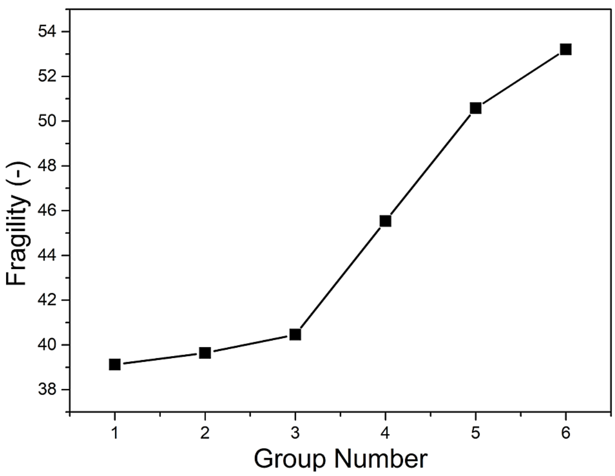

Figure 6. The fragility index of the glasses calculated by the MYEGA equation.

Relationship between the Fragility and NBO/T

The fragility reflects the glass' mid-range structure and is related to other properties [52-54]. Meanwhile, the influence of the NBO on the structure is more important than the BO in mid-range structures [24]. So, the relationship between the fragility and NBO/T is established to link the MD and the experiment. As shown in Figure 7, the linear relationship between them can be expressed as: (y is fragility). R^2 indicates the proportion of variability accounted for by the model is 0.936, which suggests a close relationship between these two variables [55]. This equation can be used to preliminarily predict the relationship between the structure and the rheological property of the glass melts.

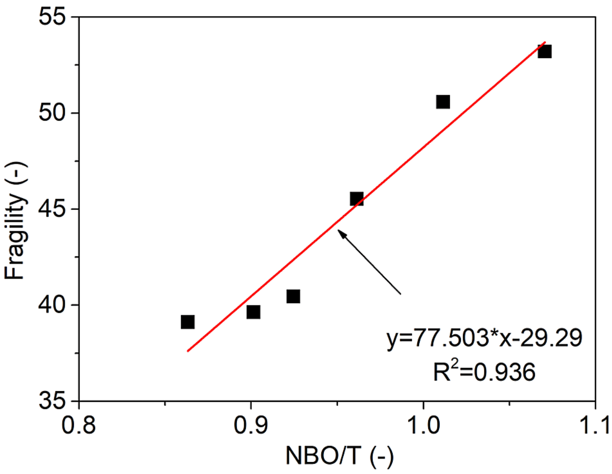

Figure 7. The linear relationship between the NBO/T and the Fragility.

CONCLUSION

In the present paper, the structures and rheological properties of Na_2O–CaO–MgO–Al_2O_3–SiO_2 glasses at high temperatures were analysed by adjusting the ratio of SiO_2/(CaO+MgO). For Si atoms, it was found that the change of $CN_{Si\text{-}O}$ was not blindingly obvious which was around 4.0. The BO content decreased from 84.5% to 64.0 % and the NBO content increased from 15.2 % to 35.0 %. The Q^4 content also declined from 37.65 % to 16.57 %. For Al atoms, the change of $CN_{Al\text{-}O}$ was glaringly significant from 4.0 to 4.2. The BO content decreased from 86.3 % to 66.0 % and the NBO content increased from 13.5 % to 32.8 %. Unlike the Si atoms, the Q^4 content of the Al atoms changed little, but its Q^3 content varied greatly from 25.00 % to 32.99 %. Meanwhile, NBO/T and BO/T were proposed to describe the polymerisation degree of the structure, where NBO/T increased from 1.298 to 1.555. Then, the melting temperature and the fragility were analysed by the MYEGA equation. The melting temperature decreased from 2030.6 K to 1723.2 K and the fragility increased from 39.12 to 53.20. Regardless of the structures or rheological properties, it indicated the depolymerisation of the glass network. Lastly, the paper discussed the relationship between the fragility and the NBO/T for describing the relationship between the mid-range structure and the rheological property. A linear relationship between them was found: $y = 77.503x - 29.29$, where R^2 was 0.9336, which showed that they were closely related.

REFERENCES

1. Donald P. J. P., Messier R. (1995): High modulus glass fibers, *Journal of Non-Crystalline Solids, 182*, 271-277. doi: 10.1016/0022-3093(94)00520-6
2. Xiao H., Cheng Y., Yu L., Liu H. (2006): A study on the preparation of CMAS glass–ceramics by in situ crystallization. *Materials Science and Engineering: A*, *431*(1-2), 191-195. doi:10.1016/j.msea.2006.05.153
3. Cavaille J.Y., Perez J., Johari G.P. (1989): Molecular theory for the rheology of glasses and polymers. *Phys Rev B Condens Matter*, *39*(4), 2411-2422. doi: 10.1103/PhysRevB.39.2411
4. Solvang M., Yue Y., Jensen S.L. (2004): The effects of Mg–Ca and Fe–Mg substitution on rheological and thermodynamic properties of aluminosilicate melts. *Journal of Non-Crystalline Solids, 345-346,* 782-786. doi: 10.1016/j.jnoncrysol.2004.08.201
5. Kjeldsen J., Smedskjaer M.M., Mauro J.C., Youngman R.E., Huang L., Yue Y. (2013): Mixed alkaline earth effect in sodium aluminosilicate glasses. *Journal of Non-Crystalline Solids,* 369, 61-68. doi: 10.1016/j.jnoncrysol.2013.03.015
6. Li S., Liu Z., Yin L., Kang J., Yue Y. (2021): The fiber spinnability and mixed alkaline effect for calcium magnesium aluminosilicate glasses. *Journal of Non-Crystalline Solids, 557*, 120643. doi: 10.1016/j.jnoncrysol.2021.120643
7. Le Losq C., Neuville D.R., Florian P., Henderson G.S., Massiot D. (2014): The role of Al^{3+} on rheology and structural changes in sodium silicate and aluminosilicate glasses and melts. *Geochimica et Cosmochimica Acta, 126*, 495-517. doi: 10.1016/j.gca.2013.11.010
8. Du J. (2015). Challenges in Molecular Dynamics Simulations of Multicomponent Oxide Glasses. In: Massobrio, C., Du, J., Bernasconi, M., Salmon, P. (eds) *Molecular Dynamics Simulations of Disordered Materials.* Springer Series in Materials Science, vol 215. Springer, Cham. doi: 10.1007/978-3-319-15675-0_7
9. Komanduri R., Raff L.M. (2001): A review on the molecular dynamics simulation of machining at the atomic scale. *Proceedings of the Institution of Mechanical Engineers, Part B: Journal of Engineering Manufacture, 215*(12), 1639-1672. doi: 10.1177/095440540121501201
10. Woodcock L.V., Angell C.A., Cheeseman P. (1976): Molecular dynamics studies of the vitreous state: Simple ionic systems and silica. *The Journal of Chemical Physics, 65*(4), 1565-1577. doi: 10.1063/1.433213
11. Soules T.F., Busbey R.F. (1983): The rheological properties and fracture of a molecular dynamic simulation of sodium silicate glass. *Journal of Chemical Physics, 78*(10), 6307-6316. doi: 10.1063/1.444556
12. Bauchy M. (2012): Structural, vibrational, and thermal properties of densified silicates: insights from molecular dynamics. *Journal of Chemical Physics, 137*(4), 044510. doi: 10.1063/1.4738501
13. Hong N.V., Ha N.T.T., Hung P.K., Iitaka T. (2019): Pressure-induced structural change of CaO–Al_2O_3–SiO_2 melt: Insight from molecular dynamics simulation. *Materials Chemistry and Physics, 236*, 121839. doi: 10.1016/j.matchemphys.2019.121839
14. Jiang C., Li K., Zhang J., Qin Q., Liu Z., Liang W., Sun M., Wang Z. (2018): The effect of CaO(MgO) on the structure and properties of aluminosilicate system by molecular dynamics simulation. *Journal of Molecular Liquids, 268*, 762-769. doi: 10.1016/j.molliq.2018.07.123
15. Jiang C., Li K., Zhang J., Qin Q., Liu Z., Liang W., Sun M., Wang Z. (2018): Molecular Dynamics Simulation on the Effect of MgO/Al_2O_3 Ratio on Structure and Properties of Blast Furnace Slag Under Different Basicity Conditions. *Metallurgical and Materials Transactions B, 50*(1), 367-375. doi: 10.1016/j.jnoncrysol.2018.06.043

16. Jiang C., Li K., Zhang J., Liu Z., Niu L., Liang W., Sun M., Ma H., Wang Z. (2019): The effect of CaO and MgO on the structure and properties of coal ash in the blast furnace: A molecular dynamics simulation and thermodynamic calculation. *Chemical Engineering Science*, *210*, 115226. doi: 10.1016/j.ces.2019.115226
17. Piao Z., Zhu L., Wang X., Xiao P., Zhou J., Wang B., Qu S., Liu K. (2020): Effect of BaO on the viscosity and structure of fluorine-free calcium silicate-based mold flux. *Journal of Non-Crystalline Solids, 542* 120111. doi: 10.1016/j.jnoncrysol.2020.120111
18. Jiang C., Xiong Z., Bu Y., Yu Y., Yu H., Li K., Liang W., Zhang J., Liu Z., Ren S. (2020): Study on the Structure and Properties of High-Calcium Coal Ash in the High-Temperature Zone of a Blast Furnace: A Molecular Dynamics Simulation Investigation. *Jom, 72*(7), 2713-2720. doi: 10.1007/s11837-020-04154-z
19. Ma J., Wang M., You J., Tang K., Lu L., Wan S., Wang J., Gong X., Wang Y. (2020): Quantitative studies on the structure of xCaO × (1 – x)SiO_2 glasses and melts by in-situ Raman spectroscopy, 29Si MAS NMR and quantum chemistry ab initio calculation. *Journal of Non-Crystalline Solids*, *546*, 120252. doi: 10.1016/j.jnoncrysol.2020.120252
20. Park J.H., Zhang L. (2020): Kinetic Modeling of Nonmetallic Inclusions Behavior in Molten Steel: A Review. *Metallurgical and Materials Transactions B*, *51*(6), 2453-2482. doi: 10.1007/s11663-020-01954-1
21. Dongol R., Wang L., Cormack A.N., Sundaram S.K. (2018): Molecular dynamics simulation of sodium aluminosilicate glass structures and glass surface-water reactions using the reactive force field (ReaxFF). *Applied Surface Science*, *439*, 1103-1110. doi: 10.1016/j.apsusc.2017.12.180
22. Tosi M.P., Fumi F.G. (1964): Ionic sizes and born repulsive parameters in the NaCl-type alkali halidesII The generalized Huggins-Mayer form. *Journal of Physics and Chemistry of Solids, 25,* 45-52. doi:10.1016/0022-3697(64)90160-X
23. Matsui M. (1994): A transferable interatomic potential model for crystals and melts in the system CaO–MgO–Al_2O_3–SiO_2. *Mineralogical Magazine, 58, 571-572.* doi: 10.1180/minmag.1994.58A.2.34
24. Jabraoui H., Badawi M., Lebègue S., Vaills Y. (2018): Elastic and structural properties of low silica calcium aluminosilicate glasses from molecular dynamics simulations. *Journal of Non-Crystalline Solids, 499*, 142-152. doi: 10.1016/j.jnoncrysol.2018.07.004
25. Plimpton S. (1995): Fast Parallel Algorithms for Short-Range Molecular Dynamics. *Journal of Computational Physic, 117,* 1-19. doi: 10.1006/jcph.1995.1039
26. Li X., Song W., Yang K., Krishnan N.M.A., Wang B., Smedskjaer M.M., Mauro J.C., Sant G., Balonis M., Bauchy M. (2017): Cooling rate effects in sodium silicate glasses: Bridging the gap between molecular dynamics simulations and experiments. *Journal of Chemical Physics, 147*(7), 074501. doi: 10.1063/1.4998611
27. Chojin K., Shimizu M., Shimotsuma Y., Miura K. (2020), Cooling-rate dependence of thermal conductivity in a sodium silicate glass: A molecular dynamics study. *Journal of the Ceramic Society of Japan, 128*(9), 656-659. doi: 10.2109/jcersj2.20039
28. Deng L., Du J. (2018): Effects of system size and cooling rate on the structure and properties of sodium borosilicate glasses from molecular dynamics simulations. *Journal of Chemical Physic, 148*(2), 024504. doi: 10.1063/1.5007083
29. Qi L., Dong L.F., Zhang S.L., Cui Z.Q., Ma M.Z., Jing Q., Li G., Liu R.P. (2008): Glass formation and local structure evolution in rapidly cooled Pd55Ni45 alloy melt: Molecular dynamics simulation. *Computational Materials Science, 42*(4), 713-716. doi: 10.1016/j.commatsci.2007.10.010
30. Xiang Y., Du J., Smedskjaer M.M., Mauro J.C. (2013): Structure and properties of sodium aluminosilicate glasses from molecular dynamics simulations. *Journal of Chemical Physic, 139*(4), 044507. doi: 10.1063/1.4816378
31. Lee J.G. (2017). *Computational Materials Science An Introduction* 2nd Ed., CRC Press.
32. Cormack A.N., Du J., Zeitler T.R. (2002): Alkali ion migration mechanisms in silicate glasses probed by molecular dynamics simulations. *Physical Chemistry Chemical Physics, 4*(14), 3193-3197. doi: 10.1039/B201721K
33. Mauroa J. C. (2009): Viscosity of glass-forming liquids. *Proceedings of the National Academy of Sciences of the United States of America*, *106* (47), 19780-19784. doi: 10.1073/pnas.0911705106
34. Deng L., Du J. (2016): Development of effective empirical potentials for molecular dynamics simulations of the structures and properties of boroaluminosilicate glasses. *Journal of Non-Crystalline Solids*, *453*, 177-194. doi: 10.1016/j.jnoncrysol.2016.09.021
35. Ren M., Lu X., Deng L., Kuo P.H., Du J. (2018): B_2O_3/SiO_2 substitution effect on structure and properties of Na_2O–CaO–SrO–P_2O_5–SiO_2 bioactive glasses from molecular dynamics simulations. *Physical Chemistry Chemical Physics*, *20(*20), 14090-14104. doi: 10.1039/C7CP08358K
36. Wang M., Anoop Krishnan N.M., Wang B., Smedskjaer M.M., Mauro J.C., Bauchy M. (2018): A new transferable interatomic potential for molecular dynamics simulations of borosilicate glasses. *Journal of Non-Crystalline Solids*, *498*, 294-304. doi: 10.1016/j.jnoncrysol.2018.04.063
37. Backhouse D.J., Corkhill C.L., Hyatt N.C., Hand R.J. (2019): Investigation of the role of Mg and Ca in the structure and durability of aluminoborosilicate glass. *Journal of Non-Crystalline Solids*, *512*, 41-52. doi: 10.1016/j.jnoncrysol.2019.03.003
38. Bouhadja M., Jakse N., Pasturel A. (2013) : Structural and dynamic properties of calcium aluminosilicate melts: a molecular dynamics study. *Journal of Chemical Physic, 138*(22), 224510. doi: 10.1063/1.4809523
39. Mongalo L., Lopis A.S., Venter G.A. (2016): Molecular dynamics simulations of the structural properties and electrical conductivities of CaO–MgO–Al_2O_3–SiO_2 melts. *Journal of Non-Crystalline Solids*, *452*, 194-202. doi: 10.1016/j.jnoncrysol.2016.08.042
40. Mazzara J.J. C., Flank A.-M., Lagarde P. (2000): Stereochemical Order around Sodium in Amorphous Silica. *Journal of Chemical Physic, 104*, 3438-3445. doi: 10.1021/jp9924474
41. Du J., Cormack A.N. (2004): The medium range structure of sodium silicate glasses: a molecular dynamics simulation. *Journal of Non-Crystalline Solids, 349*, 66-79. doi: 10.1016/j.jnoncrysol.2004.08.264
42. Jonathan Q.Z., Stebbins F. (2000): Cation ordering at fluoride sites in silicate glasses a high-resoution 19F NMR study. *Journal of Non-Crystalline Solids*, *262*, 1-5. doi: 10.1016/S0022-3093(99)00695-X
43. Xuan W., Wang H., Xia D. (2019): Depolymerization me-chanism of CaO on network structure of synthetic coal slags. *Fuel Processing Technology*, *187*, 21-27. doi: 10.1016/j.fuproc.2019.01.005

44. Maekawa H., Maekawa T., Kawamura K., Yokokawa T. (1991): The Structural Groups of Alkali Silicate Glasses Determined from Silicon-29 Mas-NMR. *Journal of Non-Crystalline Solids*, *127*(1), 53-64. doi: 10.1016/0022-3093(91)90400-Z
45. Matson D.W., Sharma S.K., Philpotts J.A. (1983): The Structure of High-Silica Alkali-Silicate Glasses. A Raman Spectroscopic Investigation. *Journal of Non-Crystalline Solids*, *58*(2-3), 323-352. doi: 10.1016/0022-3093(83)90032-7
46. Norimasa Umesaki M.T., Tatsumisago M., Minami T. (1996): Raman spectroscopic study of alkali silicate glasses and melts. *Journal of Non-Crystalline Solids*, *205-207*, 225-230. doi: 10.1016/S0022-3093(96)00439-5
47. Kuryaeva R.G. (2009): Effect of pressure on the refractive index and relative density of the $CaO·Al_2O_3·6SiO_2$ glass. *Journal of Non-Crystalline Solids*, 355(3), 159-163. doi: 10.1016/j.jnoncrysol.2008.11.020
48. Xie J., Tang H., Wang J., Wu M., Han J., Liu C. (2018): Network connectivity and properties of non-alkali aluminoborosilicate glasses. *Journal of Non-Crystalline Solids*, 481, 403-408. doi: 10.1016/j.jnoncrysol.2017.11.023
49. Sun C.-y., Liu X.-h., Li J., Yin X.-t., Song S., Wang Q. (2017): Influence of Al_2O_3 and MgO on the Viscosity and Stability of $CaO–MgO–SiO_2–Al_2O_3$ Slags with CaO/SiO_2 = 1.0. *ISIJ International*, *57*(6), 978-982. doi: 10.2355/isijinternational.ISIJINT-2016-235
50. Kreidl K.A.N. (1948): Stability of lead glass and rolarization of ions. *Journal of the American Ceramic Society*, *31*(4), 105-114. doi: 10.1111/j.1151-2916.1948.tb14273.x
51. Angell C.A. (1991): Relaxation in liquids, polymers and plastic crystals – strong&fragile patterns and problems. *Journal of Non-Crystalline Solids*, *131-133*, 13-31. doi: 10.1016/0022-3093(91)90266-9
52. Tanaka H. (2005): Relationship among glass-forming ability, fragility, and short-range bond ordering of liquids. *Journal of Non-Crystalline Solids*, *351*(8-9), 678-690. doi: 10.1016/j.jnoncrysol.2005.01.070
53. Angell C.A. (1995): Formation of glasses from liquids and biopolymers. *Science, 267*(5206), 1924-35. doi: 10.1126/science.267.5206.1924
54. Yan L., During G., Wyart M. (2013): Why glass elasticity affects the thermodynamics and fragility of supercooled liquids. *Proc Natl Acad Sci U S A*, *110*(16), 6307-12. doi: 10.1073/pnas.1300534110
55. Hrma P. (2008): Arrhenius model for high-temperature glass-viscosity with a constant pre-exponential factor. *Journal of Non-Crystalline Solids*, *354*(18), 1962-1968. doi: 10.1016/j.jnoncrysol.2007.11.016